From dimers to collective dipoles: Structure and dynamics of methanol/ethanol partition by narrow carbon nanotubes

Jose A. Garate and Tomas Perez-Acle

Citation: The Journal of Chemical Physics **144**, 064105 (2016); doi: 10.1063/1.4941331
View online: http://dx.doi.org/10.1063/1.4941331
View Table of Contents: http://scitation.aip.org/content/aip/journal/jcp/144/6?ver=pdfcov
Published by the AIP Publishing

From dimers to collective dipoles: Structure and dynamics of methanol/ethanol partition by narrow carbon nanotubes

Jose A. Garate[1,a] and Tomas Perez-Acle[1,2]
[1]*Computational Biology Laboratory, Fundación Ciencia and Vida, Santiago, Chile*
[2]*Centro Interdisciplinario de neurociencia de Valparaiso, Universidad de Valparaiso, Valparaiso, Chile*

(Received 9 November 2015; accepted 22 January 2016; published online 11 February 2016)

Alcohol partitioning by narrow single-walled carbon nanotubes (SWCNTs) holds the promise for the development of novel nanodevices for diverse applications. Consequently, in this work, the partition of small alcohols by narrow tubes was kinetically and structurally quantified via molecular dynamics simulations. Alcohol partitioning is a fast process in the order of 10 ns for diluted solutions but the axial-diffusivity within SWCNT is greatly diminished being two to three orders of magnitude lower with respect to bulk conditions. Structurally, alcohols form a single-file conformation under confinement and more interestingly, they exhibit a pore-width dependent transition from dipole dimers to a single collective dipole, for both methanol and ethanol. Energetic analyses demonstrate that this transition is the result of a detailed balance between dispersion and electrostatics interactions, with the latter being more pronounced for collective dipoles. This transition fully modifies the reorientational dynamics of the loaded particles, generating stable collective dipoles that could find usage in signal-amplification devices. Overall, the results herein have shown distinct physico-chemical features of confined alcohols and are a further step towards the understanding and development of novel nanofluidics within SWCNTs. © *2016 AIP Publishing LLC.* [http://dx.doi.org/10.1063/1.4941331]

I. INTRODUCTION

Carbon derived particles such as Carbon nanotubes (CNTs)[1] have been proposed for application in many fields ranging from electronics to medicine.[2–5] One of those, the novel field of nanofluidics[6] which studies the fluxes of atoms and molecules across nanopores and nanochannels holds the potential for the development of efficient and cheap nanodevices.[2,7–13] Moreover, CNTs offer a simplistic model system allowing for the generation of analytical theories that aim towards the description of more complex structures, inherently present in nature, e.g., membrane channels.[14–17] Among many potential applications of nanofluidic devices, the partitioning/filtration of polar molecules, i.e., alcohols from the aqueous solution is of vital importance in industry, as these species are very hard to separate due to their hydrophilic nature.[18,19] Moreover, many water pollutants possess phenolic moieties with an ongoing concern on their effects on the environment and human health.[20] In fact, many efforts are currently being carried out to develop cheap alcohol nano-filtering devices. Overall, the use of carbon nanotubes increases the selectivity towards organic alcohols such as ethanol, butanol, and isopropyl alcohol.[13,21,22]

At the nanoscale level, the continuous description for hydrodynamics fails, i.e., Navier-Stokes equations, as the flux is dominated by the movement of discrete particles.[23] Since the first reports of molecular dynamics (MD) simulations of water penetration across single-walled carbon nanotubes (SWCNTs),[24,25] it became evident that MD offered the correct description of fluxes at the molecular level; the latter is supported by the vast amount of studies which have explored this phenomenon employing both equilibrium and non-equilibrium MD simulations[26,27] and experimental validation.[28–30] Regarding water, single-file diffusion across narrow (6,6) or (5,5) SWCNTs has been thoroughly reported in the literature.[26,27] Not withstanding the hydrophobic nature of SWCNTs, an interplay between dipolar interactions plus rotational and diffusional effects is present, rendering water partitioning both energetically and entropically driven processes.[23,31–35] Meanwhile, the interaction between CNTs and other solvents has been scarcely explored and only recently, reports of alcohol separation by CNTs have appeared in the literature.[19,36–43] Small alcohols such as ethanol and methanol share common features with water, having a polar OH group and presenting a dipole; therefore, it is not strange that carbon-nanotubes do partition alcohols from an aqueous phase given the common features shared with water, plus the additional hydrophobicity provided by the carbon backbone.

Consequently, in this work, MD simulations of SWCNT ((6,6), (7,7), and (8,8)) assisted partitioning of ethanol and methanol were performed; a fully characterization based on dynamical (rotational relaxation, diffusional, mean residence times) and structural properties (interaction energies, dipolar alignment, and displacement correlations) was carried out and compared with simulations of water and methane infiltration, taken as examples of the limiting conditions of small fully polar and hydrophobic molecules, respectively. Overall, our results allowed for a detailed description of the underlying molecular mechanisms involved in alcohol partitioning by narrow SWCNTs. In brief, small alcohols form a single-file structure in narrow pores in a very similar fashion to water.

[a]Author to whom correspondence should be addressed. Electronic mail: jgarate@dlab.cl

Furthermore, the dipolar alignment normally seen in water highly depends on the SWCNT diameter, with the formation of methanol and ethanol dipole dimers in the (6,6) and (7,7) SWCNTs, respectively, and a collective dipole configuration for methanol and ethanol in the (7,7) and (8,8) SWCNTs, respectively. Even though the spontaneous partition is a very fast process (tens of nanoseconds for diluted solutions), the mobility within the SWCNTs is very slow when compared to water. Estimations based on diffusional properties and stochastic modeling evidenced that mean residence times where up to 2–3 orders of magnitude larger with respect to water, a clear consequence of the hydrophobic interaction between the pore and the alcohol carbons. The results presented herein are a further step towards the understanding of confined alcohols, providing fundamental knowledge to support the design of novel nanodevices. To achieve this goal, both a structural (or a thermodynamical) characterization and a dynamical picture are of surmount importance, specially if the aforementioned devices are intended for filtration/separation applications.

II. METHODS

A. Molecular dynamics simulations

The majority of classical MD studies utilizing standard force fields (FFs), e.g., CHARMM,[44] AMBER,[45] GROMOS[46] have employed either strong positional restraints or constraints when simulating SWCNTs.[19,26,27,36–42] Thus, the tube models are a representation of a rigid hydrophobic/aromatic pore. Similarly, in our work, the tubes are rigid (see Fig. 1 of the supplementary material[47]). The latter is because current biocompatible FFs (such as the GROMOS FF[46]) were not parametrized to adequately represent the mechanical properties of carbon allotropes. In fact, more sophisticated potential energy functions have been developed to study such properties.[48,49] In this way, to maintain the tube geometry, SWCNT's bonds and angles were constrained via Shake[50] and improper torsions were employed to impose planarity on the rings.

Many studies have shown that the filling of tubes with water is extremely sensitive to the water-carbon potential.[25,31,33–35] The Lennard Jones (LJ) values employed in the literature for ϵ_{C-OW} and σ_{C-OW} range from 0.3135 to 0.6270 kJ/mol and from 0.3190 to 0.3296 nm, respectively.[51] In this work, the LJ values for the water-carbon interaction were $\epsilon_{C-OW} = 0.5137$ kJ/mol and $\sigma_{C-OW} = 0.3262$ nm, which are in line with values used in the literature and very close to seminal works in the field.[25] In a previous study,[23] the same parameters were utilized for rigorous free-energy calculations of the SPC (Single Point Charge) water-loading process, which were in good agreement with other theoretical studies[31,33–35] and the experimental evidence that water fills these hydrophobic channels.[28–30] Regarding the tube carbons and alcohol carbons interactions, up to our knowledge, no detailed comparison or overview of LJ parameters employed in the literature exists. Nevertheless, other authors have shown that no qualitative differences are observed for alcohol partition when different parameter sets are employed.[41] In Table 1 of the supplementary material,[47] an overview of all the LJ parameter and partial charges of the simulated molecules is shown.

MD simulations were performed using the GROMOS11 simulation package.[52,53] All bonds and angles were constrained to their reference values employing the SHAKE algorithm[50] with a relative tolerance of 10^{-4}, permitting a time step of 2 fs via the leapfrog algorithm.[54] Periodic boundary conditions in a cubic box were applied. A triple range cutoff scheme was utilized to compute non-bonded interactions; within a short-range cutoff of 0.8 nm, interactions were computed every time-step, from a pair-list updated every 5 steps. At these time points, interactions between 0.8 and 1.4 nm were also computed and kept constant. A reaction-field contribution was added to Coulombic interactions, akin a homogeneous medium outside the long-range cutoff, employing the relative permittivity of SPC water (61).[55] All interactions were calculated using the GROMOS 45A4 FF.[46] After a steepest-descent minimization to remove bad contacts, velocities were randomly assigned from a Maxwell-Boltzmann distribution at 298 K. All production runs were simulated at the canonical (NVT) ensemble using the Nosé–Hoover chains coupling algorithm for temperature control (3 chains, 298 K).[56,57] The SWCNT and solvent/solute atoms were independently coupled to the heat bath.

Open (6,6), (7,7), and (8,8) SWCNTs of lengths 3.19 nm and widths of 0.8, 0.9, and 1.0 nm, respectively, were placed in a $5.3 \times 5.3 \times 5.3$ nm^3 SPC box. Subsequently and after equilibration, randomly selected water molecules were replaced by solute molecules (methane, methanol, or ethanol) in the solvent box until reaching the desired concentration (see Fig. 1); for each solute, four concentrations were evaluated, specifically 0.25, 0.50, 1.0, and 2.0 mol/L, which for the simulated volumes accounted for 20, 50, 100, and 200 molecules, respectively. Each system, on an average, comprised a total number of 4500 atoms. A depiction of a (6,6) SWCNT in water/methanol mix is shown in Fig. 1.

The tubes were free to diffuse along the periodic box. For ease of calculations and posterior analyses, all trajectories were submitted to a RMSD (Root-Mean-square Deviation) fit to a tube with its main axis aligned in the z direction. Initially, all systems were simulated until filling was obtained, defined as the average load number for the 0.25 molar systems,

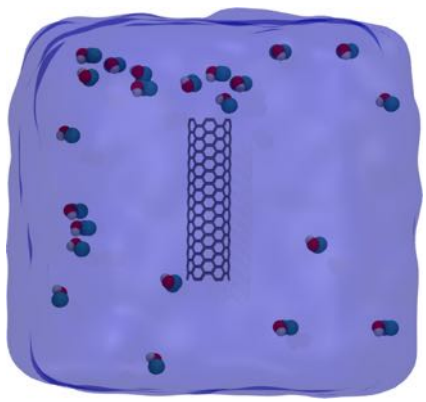

FIG. 1. Example of one of the simulated systems: a (6,6) SWCNT solvated in a 0.25M methanol/water solution.

which normally lasted less than 15 ns. Three independent replicas were run for each alcohol concentration. Simulations at 0.25 mol/L were extended to 50 ns for further analysis; the control simulations (water and methane) were run for 25 and 50 ns, respectively. Overall, 1.3 μs of simulation time was performed.

B. Selectivity

The selectivity f_{sel}[42] of a given SWCNT to different alcohols was defined as

$$f_{sel} = R_{SWCNT}/R_{bulk}, \tag{1}$$

where R_{SWCNT} and R_{bulk} are the ratios of the average numbers of alcohol molecules to water in the tube and in the bulk, respectively.

C. Diffusion coefficients

Self-diffusion coefficients along the pore axis (D_z) for the oxygen of SPC water, methane carbon, and center of mass (COM) of methanol and ethanol were calculated from mean-squared displacements (MSDs), using the Einstein relation,[58]

$$D_z = \lim_{t\to\infty} \frac{\langle (r_z(t_0+t) - r_z(t_0))^2 \rangle_{t_0}}{2t}, \tag{2}$$

where $r_z(t)$ corresponds to the z component of the particle position vector (only located within the pore) at time t, and the averaging is performed over multiple time origins (t_0) and loaded molecules. Albeit there is an open discussion regarding the validity of Eq. (1) in confined geometries,[59,60] several reports and our previous work[10,23] have shown that for open tubes, the flux is fickian along the pore main axis.

D. Reorientational relaxation

Particles orientation inside the pore region was described by

$$P_1 = \frac{\vec{\mu}_i}{|\vec{\mu}_i|} \cdot \hat{k} \tag{3}$$

and a collective P_{1coll} of all loaded molecules,

$$P_{1coll} = \left(\sum_i^n \frac{\vec{\mu}_i}{|\vec{\mu}_i|} \right) \cdot \hat{k}, \tag{4}$$

where $\vec{\mu}_i$ is the dipole of the ith molecule, and $\hat{k}$ is a unitary vector pointing along the tube main axis direction.

For this vector ($\frac{\vec{\mu}_i}{|\vec{\mu}_i|}$) and a vector perpendicular to $\frac{\vec{\mu}_i}{|\vec{\mu}_i|}$ (for SPC water, this is the vector that connects both hydrogens atoms; for methanol and ethanol, we chose the vector along the oxygen-carbon bond, which forms a angle of 108° with the dipole angle, being closely perpendicular to the dipole vector and almost parallel the tube radial plane), we computed reorientation correlation functions $C_\alpha(t)$ of SPC water, methanol, and ethanol,

$$C_\alpha(t) = \langle \hat{e}_\alpha(t) \cdot \hat{e}_\alpha(t_0) \rangle_{t_0}, \tag{5}$$

where $\hat{e}_\alpha$ is a unit vector pointing along the direction of the α axis, the angular brackets denote average over loaded particles and multiple time origins. $C_\alpha(t)$ normally shows an exponential decay and can be fitted employing the following expression:

$$C_\alpha(t) = A \exp\left(\frac{-t}{\tau_\alpha}\right), \tag{6}$$

where τ_α denotes the first-order rotational relaxation time and A is a constant. Reorientational times of the collective versions of the above vectors (see Eq. (4)) were also computed.

E. Mean residence times

An important quantity characterizing the dynamics of confined molecules is the survival probability of the particles within the nanotube boundaries.[61] This probability was computed employing the definition,

$$Q(t) = \sum_{i=1}^{N} \left\langle \prod_{t_k=t_0}^{t_0+t} P_i(t_k) \right\rangle, \tag{7}$$

where P_i is defined such that it equals 1 if particle i is located inside the pore at time t or zero otherwise. The summation is over all the loaded molecules and the angular brackets denote an average over multiple time origins, t_0. Generally, the survival probability is normalized to unity by dividing it by its value at t = 0. $Q(t)$ defines the probability that a particle remains inside the pore for all times between t_0 and $t_0 + t$, averaged over multiple time origins. The distribution of residence times for all loaded particles, $p(t)$, is related to $Q(t)$ in the following way:[61]

$$Q(t) = \frac{\int_t^{tm} (t' - t) p(t') dt'}{\int_0^{tm} p(t') dt'}. \tag{8}$$

Normally, residence times decay exponentially with time. If so, then $Q(t)$ would also decay exponentially with the same time scale time at long times. Therefore, mean residence times can be obtained by fitting $Q(t)$ employing the following expression:

$$Q(t) = A \exp\left(\frac{-t}{\tau_s}\right), \tag{9}$$

where τ_s is the average residence time.

F. Displacement correlation

The displacement correlation between neighboring particles was quantified employing the following expression:[61]

$$\Delta z_c = \langle \delta z_i(\delta t) \delta z_j(\delta t) \rangle_{t_0}, \tag{10}$$

where $\delta z_i(\delta t)$ and $\delta z_j(\delta t)$ are the displacements along the pore axis of the i-th and j-th particles, in a time interval of δt. The angular brackets denote an average over loaded particles and multiple time origins. The chosen time interval employed in Eq. (10) was of 1 ps.

G. Kinetic Monte Carlo (KMC) simulations

KMC simulations based on the scheme of Kalra *et al.*[36] were carried out in order to compute mean residence times

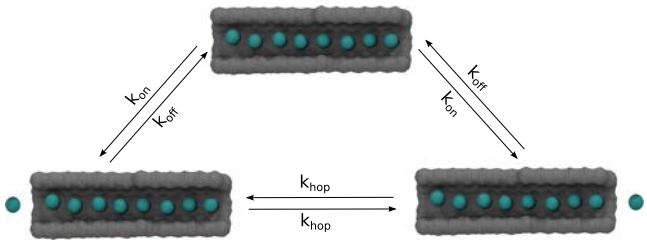

FIG. 2. Kinetic model employed for the KMC simulations; k_{hop}, k_{on}, and k_{off} which are the rate coefficients for hopping, association, and dissociation, respectively.

for single-file diffusion. In this very simple model, three parameters need to be defined: k_{hop}, k_{on}, and k_{off} which are the rate coefficients for hopping, association, and dissociation, respectively, and were computed as follows[14] (see Fig. 2):

$$k_{off} = k_{hop} = \frac{2D_z}{a^2}, \tag{11}$$

where D_z is the axial diffusion coefficient computed from Eq. (2) and a is the average spacing between loaded molecules, defined as the average load divided by the tube length ($\langle N \rangle / L$). k_{on} is related to the diffusion of molecules within the vicinity of the pore, calculated from the diffusion-controlled rate coefficient,[36]

$$k_{on} = 4\pi R^* D \rho, \tag{12}$$

where R^* is the radius of a hemispherical region surrounding the pore mouth, in this work defined to be 0.6 nm; D is the diffusion coefficient of the solute molecule in SPC water; and ρ is the number density of the solute. Please refer to Table 2 of the Supplementary material[47] for the actual numbers employed in this work. A graphical description of the aforementioned scheme is depicted in Fig. 2.

III. RESULTS AND DISCUSSION

All results presented below are averages over the three independent 0.25 mol/L simulations, unless stated otherwise.

A. Filling kinetics

All simulations started with empty tubes. The water filling process is faster; thus, in all cases, water initially fills the tube and then is replaced by solute molecules (methanol and ethanol). The filling kinetics of alcohol partitioning by SWCNTs, i.e., the time required to achieve filling was monitored and quantified as seen in Fig. 3. Overall, the process is fast and no substantial differences between methanol and ethanol are observed. Rough estimations assuming a diffusion-limited process of a single particle according to Eq. (12) times the average load of each tube (see dashed lines of Fig. 3) are considerably lower compared to the times obtained in MD simulations. The latter indicates that the pore entry-kinetics plays a role, not to mention that the tube cavity is already solvated; in other words, a replacement and competition with water molecules, i.e., pore re-entry takes place, explaining the aforementioned differences. At higher concentrations, this

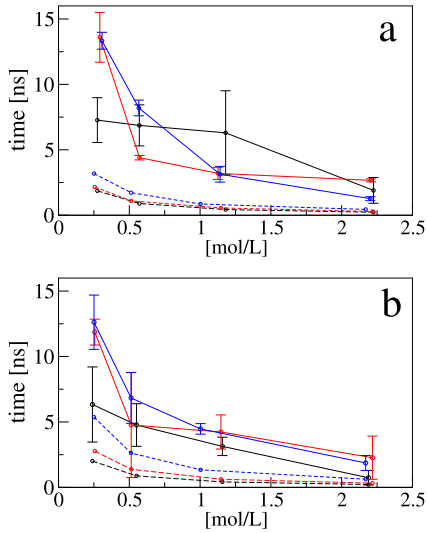

FIG. 3. Filling kinetics as function of solute concentration. Each point is the average filling-time (over three independent simulations). In black, red, and blue, the (6,6), (7,7), and (8,8) systems, respectively; in dashed lines, filling-time estimations assuming a diffusive-limited process. (a) Methanol partitioning; (b) ethanol partitioning.

is not the case as the alcohol particles can readily fill the pore, leaving only the pore-entry kinetics as the limiting step. Indeed, the entry kinetics can be estimated by hopping rates k_{hop} (see Eq. (11)) inside the tube; for ethanol and methanol, these are in the order of 0.1 ns, which multiplied by the average loads (≈10, see Table I) gives a filling duration of about 1–3 ns, in fair agreement with the times obtained at high concentrations.

B. Selectivities and single-file structure

In Table I, average loads and selectivities are presented. When compared to methane, the selectivities towards alcohols are considerable lower; however, it is important to note that methane fully excludes water from the tubes, rendering f_{sel} to infinity (see Eq. (1)). Consequently, the polar nature of both methanol and ethanol increases the water content and notoriously reduces the selectivity towards these alcohols. As expected, the SWCNT diameter is a key factor, with the (8,8) and (7,7) pores being more selective to ethanol. On the other hand, the (6,6) pore presents a higher f_{sel} for methanol with respect to ethanol, which is not strange due to the inherent geometric restraints of this narrow pore. Interestingly, some systems show a systematic water content, specifically the methanol-loaded (8,8) and (7,7) tubes and the ethanol-loaded (6,6) pore (see Figs. 4 and 5 of the supplementary material[47]) structural considerations fully explain the above facts and will be thoroughly discussed in the following paragraph.

To gain further insight into the structural details of alcohol partitioning, 2D atomistic density profiles along the radial-axial plane, i.e., z-axis plane, are shown in Fig. 4 for one 0.25 mol/L simulation; the other two replicas are shown in Figs. 4 and 5 of the supplementary material[47] in the form of 1D axial profiles for methanol and ethanol, respectively. The 2D profiles for water and methane are shown in Fig. 2 of the supplementary material.[47]

TABLE I. Average loads and selectivities.

SWCNT			
(6.6) 0.25 mol/L			
Molecule	$\langle N\rangle_A$[a]	$\langle N\rangle_W$[b]	f_{sel}[c]
H_2O (SPC)	...	11.54 ± 0.01	...
CH_4	7.94 ± 0.01	0.00 ± 0.00	$1.7\times10^6\pm0.44$
CH_3OH	7.66 ± 0.26	0.09 ± 0.02	$1.7\times10^4\pm0.26$
CH_3CH_2OH	4.58 ± 0.38	1.79 ± 0.68	552.91 ± 0.38
(7.7) 0.25 mol/L			
Molecule	$\langle N\rangle_A$	$\langle N\rangle_W$	f_{sel}
H_2O (SPC)	...	20.40 ± 0.06	...
CH_4	9.38 ± 0.08	0.03 ± 0.01	$5.9\times10^4\pm0.30$
CH_3OH	9.59 ± 0.44	3.07 ± 0.88	560.72 ± 0.29
CH_3CH_2OH	6.46 ± 0.73	1.51 ± 2.60	858.78 ± 1.72
(8.8) 0.25 mol/L			
Molecule	$\langle N\rangle_A$	$\langle N\rangle_W$	f_{sel}
H_2O (SPC)	...	40.13 ± 0.09	...
CH_4	16.21 ± 0.09	0.10 ± 0.01	$2.6\times10^4\pm0.09$
CH_3OH	14.69 ± 0.09	8.37 ± 1.10	299.15 ± 0.02
CH_3CH_2OH	12.89 ± 0.15	0.29 ± 0.10	$9.2\times10^3\pm0.36$

[a]Average alcohol load.
[b]Average water load.
[c]Selectivity.

Similar to water (see Figs. 1 and 2 in the supplementary material[47]), a single-file structure with alcohol molecules forming 1D chains is clearly observed; however, the details of these configurations are very sensitive with respect to the pore width and the loaded particle. For example, methanol forms a single-file in both the (6,6) and (7,7) SWCNTs, for the wider (8,8) tube, this is not the case, and a "ring-shaped" formation takes place, a clear consequence of the wider SWCNT diameter allowing enough room for two molecules to be located along the sections of the tube, as previously reported by Zhao *et al.*[41] Interestingly, the (6,6) and (7,7) configurations are quite different, in fact, the more canonical form only occurs in the (7,7) pore where the typical h-bonded chain is present (see Fig. 6 of the supplementary material[47]);[16] on the other hand, a dimer formation is appreciated within the (6,6) tube, as a consequence of its smaller diameter which clearly hinders the proper formation of the h-bond chain (see Fig. 6 of the supplementary material[47]). The dipolar configurations are very distinctive, with dimers forming independent dipoles that do not necessarily align in the same direction (see Fig. 4, first column, first row); in contrast, a continuous dipole chain, i.e., a collective dipole, is readily observed for the (7.7) methanol-loaded pores (see Fig. 4, first column, second row). Moreover, water molecules intercalate in between the gaps of neighboring methanol molecules, further enhancing the formation of the collective dipole (see also Fig. 4 of the supplementary material). Likewise, ethanol forms dimers within the (6,6) and (7,7) pores as well, with the continuous chain only present in the (8,8) tube; in this case, no water intercalation occurs. The "ring-shaped" formation of methanol in the (8,8) pores pertains to the same phenomenon, with now two collective dipoles in an "up-down" configuration. Interestingly, for ethanol, we did observe a regular water intercalation, specially for the (6,6) pore (see Fig. 4, second column, first row, and Fig. 5 of the supplementary material[47]). A visual inspection of these simulations revealed that loaded water molecules were trapped between ethanols that penetrated from opposing faces of the tube, forming a heterogeneous tetramer with two molecules of each species.

From these considerations, the selectivities shown in Table I can be rationalized; for methanol, when a collective dipole is formed, water molecules can easily become part of such arrangements via h-bonding, reducing the energetic penalty due to hydrophobic confinement. On the contrary (for both methanol and ethanol), when dimers are present, the inter-space among these is flanked by carbon atoms, thus hindering water intercalation. The consistent water content for the ethanol-loaded (6,6) pore derives from the placement of water molecules in between the ethanol dimers; thus, water becomes kinetically trapped within the pore. No water infiltration is observed for the (8,8) pores, and in this way, even though the collective arrangement is formed, ethanol fully displaces water.

Previous works have rationalized alcohol selectivity, in particular, for methanol, on the light of van der Waals (VdW) interactions with the SWCNT walls plus h-bonding among loaded particles.[41] In detail, the main driving force for alcohol partitioning comes from the interaction with tube atoms; in other words, it is proportional to r^2, being r the pore radius. However, the inner pore volume increases by r^3, that is why, in general, the selectivity decreases with the pore diameter;[41] this is clearly the case for the methanol-loaded SWCNT in which a higher volume shifts carbon towards the pore walls allowing water intercalation (at high concentrations, a lower water content for the (8,8) pore is expected, as shown in Ref. 41). However, all these arguments have partially ignored the electrostatic contribution that arises when a collective dipole is formed. Indeed, the slight increment of the ethanol selectivity towards the (8,8) SWCNT seems to be in part due to such interaction, at least at these low concentrations. We will further examine the structural and energetic properties of this so called dimer to collective dipole transition and its repercussions regarding the dynamical properties of the loaded particles.

C. Dimeric to collective dipole transition

As shown in Sec. III B, the level of confinement triggers a structural transition from dimers towards a single-file configuration including a collective dipole. A graphical depiction of the later is shown in Fig. 5 as 2D density profiles comprising the radial dimensions (i.e., x and y axes) of the inner tube section, averaged over the axial axis. For completeness, 2D profiles for water and methane are also shown in Fig. 3 of the supplementary material.[47] Atomic-wise, when a canonical single-file structure (or collective dipole(s)) is present, e.g., the methanol-loaded (7,7) and ethanol-loaded (8,8) SWCNT, carbon atoms tend to locate in close contact

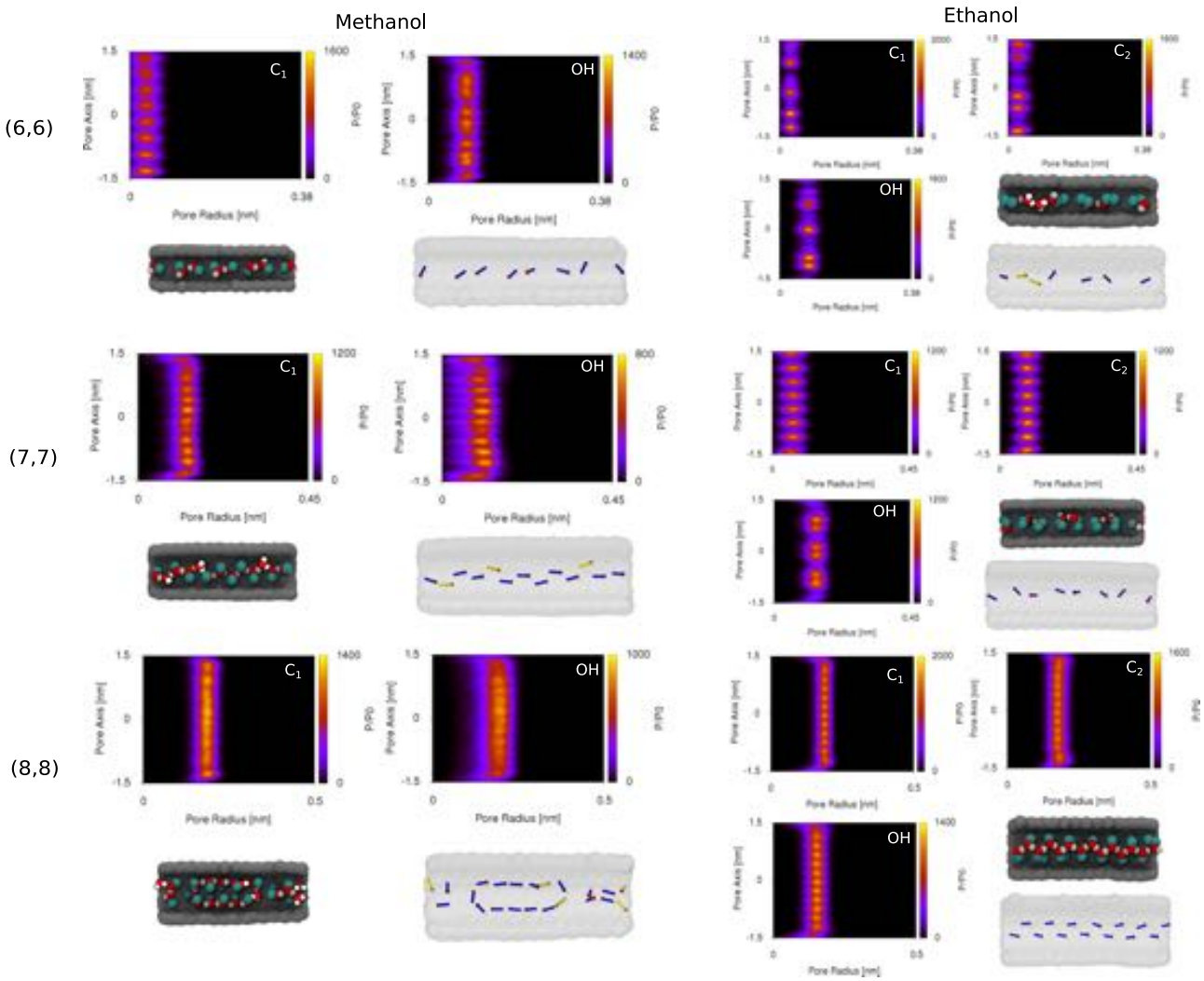

FIG. 4. Axial (z axis)-radial atomic density profiles for alcohol partition at 0.25 mol/L concentration for a single extended simulation; rows 1, 2, and 3, the (6,6), (7,7), and (8,8) SWCNTs, respectively; 1st and 2nd columns, the methanol and ethanol profiles, respectively; below each set of density profiles, a representative MD snapshot with its corresponding dipolar configuration. In gray, cyan, red, and white tube carbons, alcohol carbons, oxygens, and hydrogens, respectively; blue arrows depict alcohol dipoles; yellow arrows depict water dipoles.

with the tube wall while the oxygen atoms tend to be centrally placed. The opposite is observed when dimers are formed, and an example of the latter is clearly appreciated for ethanol-loaded (7,7) pores (see second row of Fig. 5). Moreover, the single file placement is helically shaped, with carbon atom(s) of contiguous particles switching sides along the tube axis. This structural transition is very sensitive to the tube and loaded-molecule dimensions, denoting a fine tunning between electrostatics and dispersion interactions that controls this transition.

Energetic analyses have anteriorly been reported for ethanol-loaded (13,13) pores in the form of VdW and Coulomb total pair interaction energy distributions;[42] it was shown that the VdW interaction is significantly enhanced in the confined state with a slight reduction in the electrostatics with respect to a bulk aqueous solution. Nonetheless, a detailed energetic characterization of the pore loading process is still missing, and ergo in Fig. 6, the average non-bonded interaction energy of loaded particles was decomposed into three pair interaction terms, each pertaining to a specific molecular species (the SWCNT, loaded water, and loaded alcohol) which were further decomposed into their VdW and Coulomb terms, and computed as function of the tube load. In Fig. 6, only the pore-alcohol VdW (red), water-alcohol Coulomb (blue), and alcohol-alcohol Coulomb (black) terms are depicted. The rest of the interaction terms are notoriously less favorable; only the water-alcohol VdW interaction is above k_BT with consistent positive values for low alcohol loads, a consequence of the tightly packed alcohol-water chain (see Fig. 8 of the supplementary material[47]).

VdW interactions become less favorable with the tube width, similarly to water (see also Fig. 9 of the supplementary material[47]),[23] and these terms are constant with values of −54.1 ± 1.2, −40.5 ± 0.5, and −33.7 ± 0.2 kJ/mol for methanol-loaded (6,6), (7,7), and (8,8) tubes, respectively. Ethanol-loaded (6,6), (7,7), and (8,8) tubes, likewise, show constant VdW terms of −79.3 ± 1.6, 62.8 ± 1.1, and −48.77 ± 1.1 kJ/mol, respectively. Moreover, the ratio of these constant terms for the same tube infiltrated with methanol or ethanol is around 1.5; thus, the enhancement of the VdW interaction tends to follow the number of heavy atoms (2 → 3) of the loaded alcohol. Previous authors have

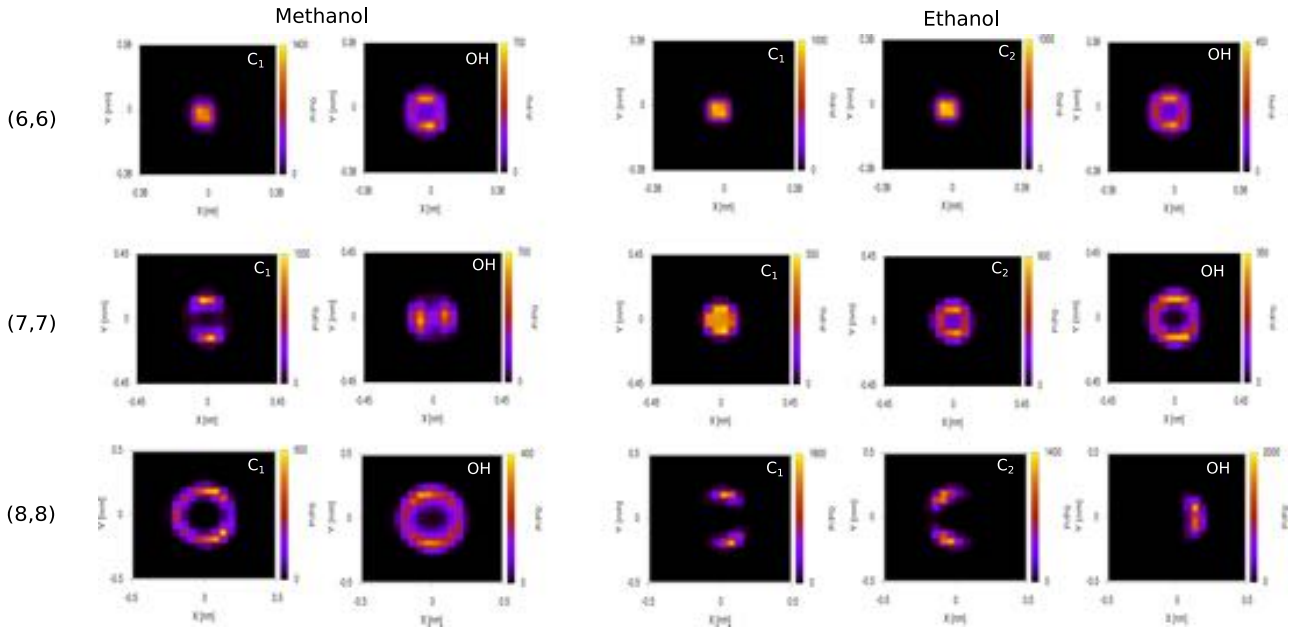

FIG. 5. x-y atomic density profiles for alcohol partition at 0.25 mol/L concentration; rows 1, 2, and 3 the (6,6), (7,7), and (8,8) SWCNTs, respectively; 1st and 2nd columns, the methanol and ethanol profiles, respectively.

modelled these interactions as effective chemical potentials in simplified lattice models, via Monte Carlo simulations.[16] For full loads, strong confinement renders VdW interactions as the dominating component, with the tube-alcohol VdW term being 4–5 times bigger than its electrostatic counterpart.

Regarding electrostatics, there is a smooth transition from a water-alcohol towards and alcohol-alcohol interaction, whereas the former is considerably higher when normalized by the alcohol/water content, and the latter is due to the strong dipole of SPC water with respect to ethanol or methanol. As described elsewhere,[23,42] there is a cooperativity effect

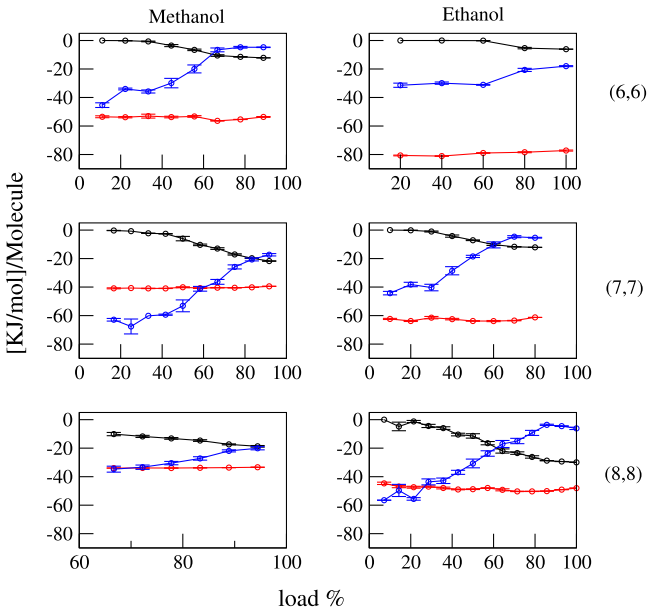

FIG. 6. Average normalized non-bonded interaction energies for loaded particle as a function of pore loading percentage. In black, Coulomb interaction with the rest of the loaded alcohol molecules; in blue, Coulomb interaction with water molecules; in red, VdW interaction with the SWCNT atoms.

with each added particle further enhancing the interaction. Interestingly, for dipole dimers of the methanol-loaded (6,6) or (7,7) and the ethanol-loaded (7,7) tubes, there is a rougher increment with each added particle; this is expected as a significant contribution only occurs when a dimer is formed. On the other hand, when a collective dipole is present, every additional molecule becomes part of it, further enhancing the electrostatic interaction with an estimated addition of 3.5 and 3.2 kJ/mol per each added particle for the methanol-loaded (7,7) and ethanol-loaded (8,8) tubes, respectively. Whereas, in the systems studied herein, the VdW terms are dominant, for longer tubes, the electrostatics should be the dominant force, given the constant nature of the VdW terms.

In this work, electronic polarization is fully neglected. Up to our knowledge, only few MD studies have reported the use of polarizable graphene/SWCNT employing, for example, the Drude particle formalism[62,63] or other approaches.[64–67] For water in contact with graphene, it has been shown that including (isotropic) polarizability has no effects on the oxygen vertical distribution, but it leads to small orientational effects, as one of the hydrogens tends to project towards the surface.[67] Likewise, Moulin *et al.*[65] demonstrated that polarization effects are maximal for water within the tubes when employing anisotropic polarizability tensors; nonetheless, they only accounted for a small percentage (8%) of the total water-tube interactions, at room temperature (298 K), and for tubes diameters and lengths of 0.8 and 2.0 nm, respectively. In this regard, no such studies have been carried out for alcohol-SWCNT interactions. Previous works have suggested that polarizability has a larger influence on liquid alcohols than water;[68] however, for confined alcohols (and water), interactions strongly depend on the molecular geometry (orientational polarization)[65] which is included in the point charge description of the GROMOS 45AA force-field.[46] Finally, VdW interactions with the tube walls dominate

the alcohol loading process, in a mean-field approximation, the latter includes induced polarization effects.

Overall, the above structural and energetic description indicates the existence of a transition from a VdW to a more electrostatic dominant process, as a function of the pore width (which should be fully dominant for longer tubes) determining the inner structure of the loaded particles, i.e., from dimers to a collective dipole. In Sec. III D, we will explore the repercussion of these confined conformations on the diffusional and reorentational dynamics of the loaded particles.

D. Diffusivities and mean residence times

Water dynamics within SWCNTs has been extensively explored.[26,27] Briefly, for a collective single-file structure, the smooth and hydrophobic pore walls generate a fast one-dimensional diffusional process, with no loss of mobility, when compared to the bulk.[14–17,25] The dynamics of confined alcohols within narrow tubes should share common features with those of confined water given their dipolar nature; nevertheless due to the presence of hydrophobic carbons, the overall dynamics will undoubtedly be perturbed when compared to confined water. In this way, Table II presents a dynamical description in the form of axial diffusion coefficients (see Eq. (2)) and mean residence times (see Eqs. (7)–(9)).

It is clear that the carbon content of both alcohols greatly reduces the mobility within the pore cavity, being at least two orders of magnitude lower compared to alcohol in aqueous solution and confined water (see Table II). With respect to confined methane, these differences are reduced but diffusivity is still smaller. For alcohols (and methane), the favorable VdW terms with the pore wall generate a frictional effect (see Fig. 6); thus, a higher carbon content should lead to lower mobilities. This tendency is observed in our simulations but the differences for both alcohols in the same tubes are within the error margins; we estimate that at higher temperatures, these differences should be more pronounced. When diffusivity is compared in light of the presence of dimers or a collective dipole, the latter seems to reduce the mobility of the loaded particles, although these differences are within the statistical error. In fact, the lower mobility (and error) of the ethanol-loaded (8,8) SWCNT points towards this direction, specially because the VdW term for this system is considerably diminished (see Fig. 6). We hypothesize that dipole dimers will tend to generate repelling forces due to the presence of opposing dipoles (see Fig. 4), incrementing the diffusivity along the axial dimension of the tube.

The mean residence times estimates from MD simulations (see Table II) are (as expected) in line with the mobility calculations. However, adequate survival probabilities calculations require simulations far above the mean residence time for proper sampling, which is certainly not the case for the majority of our simulations, due to their slow diffusivity within the tubes; In truth, not a single permeation event was recorded for the majority of the alcohol-loaded simulations. Given these circumstances, mean residence times estimates were calculated from a simplified kinetic model via KMC simulations (see Fig. 2). The KMC simulations accuracy was assessed for the (6.6) pores loaded with water and methane, where the fast mobilities of the infiltrated particles allow for a fair comparison with the MD estimates (see Eq. (9)). The KMC-derived mean residence time estimates are in close agreement with the MD calculations (see Table II); however, other authors have shown in light of analytical models based on a simplified diffusion equation, better agreement regarding water mean residence times in (6,6) tubes.[61] The latter is expected, as these models employ less simulation derived parameters, besides these simulations were performed with fixed pores, which resembles more the models employed to derive such formulations.[14,17,61]

The alcohols mean residence times from the KMC simulations range from 15 to 84 ns with very high survival times for single-file ethanol-loaded tubes (see Table II). Still,

TABLE II. Diffusivity of confined alcohols.

SWCNT			
(6.6) 0.25 mol/L			
		Mean residence time (ns)	
Molecule	D_z (nm^2/ns)[a]	MD[b]	KMC[c]
H_2O (SPC)	3.49 ± 0.53	0.25 ± 0.04	0.14 ± 0.00
CH_4	0.13 ± 0.02	11.85 ± 0.20	11.20 ± 0.00
CH_3OH	0.04 ± 0.01	…[d]	18.79 ± 0.00
CH_3CH_2OH	0.03 ± 0.02	…	32.49 ± 0.00
(7.7) 0.25 mol/L			
		Mean residence time (ns)	
Molecule	D_z (nm^2/ns)	MD	KMC
H_2O (SPC)	0.86 ± 0.15	0.69 ± 0.93	*[e]
CH_4	0.07 ± 0.02	…	15.89 ± 0.00
CH_3OH	0.04 ± 0.02	…	17.38 ± 0.00
CH_3CH_2OH	0.02 ± 0.01	…	55.63 ± 0.00
(8.8) 0.25 mol/L			
		Mean residence time (ns)	
Molecule	D_z (nm^2/ns)	MD	KMC
H_2O (SPC)	0.51 ± 0.02	1.16 ± 0.11	*
CH_4	0.90 ± 0.03	2.20 ± 1.01	*
CH_3OH	0.11 ± 0.01	9.00 ± 0.83	*
CH_3CH_2OH	0.01 ± 0.00	…	84.34 ± 0.02
Bulk SPC			
Molecule	D (nm^2/ns)[f]		
H_2O (SPC)	4.00 ± 0.00		
CH_4	3.50 ± 0.00		
CH_3OH	3.30 ± 0.00		
CH_3CH_2OH	2.10 ± 0.00		

[a]Axial diffusion coefficient.
[b]Mean residence time estimate from MD simulations.
[c]Mean residence time estimate from KMC simulations.
[d]Unreliable estimate from MD.
[e]Multi-load system, KMC model is not applicable.
[f]Diffusion coefficient.

the kinetic model of Fig. 2 defines particle displacement as a fully correlated motion; thus to explore the validity of this strong assumption, displacement correlations along the pore axis for single-file systems were calculated via Eq. (10) and are shown in Fig. 7. Overall, correlations are proportional to the confinement level with alcohols presenting much lower correlations with respect to either water or methane (see Fig. 10 of the supplementary material[47]); thus, KMC derived data should be taken only as rough estimates and are expected to vary more than its methane or water counterparts. Indeed, a further assumption of this simplified model involves the equality of k_{hop} and k_{off}; in previous work, we have shown that this not necessarily true for water.[9] In truth, we expect that for alcohols, a significant barrier for the pore exit process exists, further differentiating k_{hop} from k_{off}.

In this manner, the KMC model estimates can serve to guide the study of systems in which low diffusivity severely hinders proper sampling of permeation events. Apart from the numerical efficiency, these models are very general only needing the calculation of few parameters in a single long MD simulation. This is because, in diluted solutions, the bulk diffusion coefficients are not altered and the diffusivity within the pore is not affected by the overall solute concentration (the diffusion coefficient for the methanol-loaded (8,8) tubes at 2.2 mol/L is 0.10 ± 0.08 nm^2/ps). Likewise, they can be easily expanded to study other conditions such as concentration gradients or membranes, as done by others.[14]

E. Rotational relaxation

The rotational symmetry is broken for confined water with rotations along the dipole axis severely augmented due to the constant exchange between dangling h-bonds with adjoining particles.[23,27] On the contrary, the strong collective dipole hinders rotations along the perpendicular dipole axis. To explore this characteristic feature for alcohol-loaded tubes, the rotational relaxation times for the dipole ($\vec{\mu}$) and a vector perpendicular to it ($\perp \vec{\mu}$), with their corresponding collective versions, coll $\vec{\mu}$ (see Eqs. (3)–(6)) were computed and are shown in Table III. In Fig. 11 of the supplementary material,[47] the distributions and time-series of the collective P1 parameter (see Eq. (4)) and the collective-dipole magnitude are also depicted.

In all cases, rotations are heavily influenced by confinement; when compared to the bulk, relaxation times for rotations along the dipole axis, in general, are enhanced, i.e., a low rotational relaxation time $\tau \perp \vec{\mu}$ and rotations along the perpendicular dipole axis are diminished, i.e., a high rotational relaxation time $\tau\mu$. Contrary to the water case, the collective configuration of both methanol-loaded and ethanol-loaded (7,7) and (8,8) tubes, respectively, also heavily hinders rotations along the dipole axis as well. As shown in Fig. 5, carbon atoms tend to locate close to the pore wall hindering these rotations due to favorable interactions with the tube atoms. On the contrary, the dimeric conformations resulted in carbon atoms placed right in the middle of the tube, resulting in a symmetric environment that leads to frequent rotations along this axis with an insignificant energetic penalty.

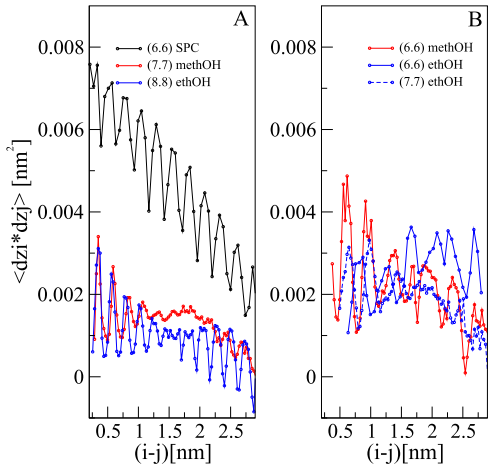

FIG. 7. Displacement correlation of loaded particles. (a) Correlations for single-files that form a collective dipole; (b) correlations for single file that form dimers.

TABLE III. Rotational relaxation of confined alcohols.

SWCNT				
(6.6) 0.25 mol/L				
	$\tau\mu$ (ps)[a]		$\tau \perp \mu$ (ps)[b]	
Molecule	μ	coll μ[c]	$\perp \mu$	coll $\perp \mu$[d]
H_2O	433 ± 183	968 ± 63	0.3 ± 0.0	0.3 ± 0.0
CH_3OH	47 ± 10	58.6 ± 9.3	0.5 ± 0.0	0.5 ± 0.0
CH_3CH_2OH	271 ± 168	148 ± 107	0.6 ± 0.3	0.4 ± 0.0
(7.7) 0.25 mol/L				
	$\tau\mu$ (ps)		$\tau \perp \mu$ (ps)	
Molecule	μ	coll μ	$\perp \mu$	coll $\perp \mu$
H_2O	72.7 ± 3.2	75.4 ± 3.1	3.5 ± 0.1	0.7 ± 0.0
CH_3OH	…[e]	…	193 ± 112	162 ± 103
CH_3CH_2OH	53.5 ± 9.9	63.9 ± 9.5	0.9 ± 0.3	0.5 ± 0.1
(8.8) 0.25 mol/L				
	$\tau\mu$ (ps)		$\tau \perp \mu$ (ps)	
Molecule	μ	coll μ	$\perp \mu$	coll $\perp \mu$
H_2O	115 ± 28	40 ± 12	49.3 ± 3.8	2.2 ± 0.0
CH_3OH	210 ± 115	673 ± 286	26 ± 11	19.1 ± 2.2
CH_3CH_2OH	…	…	…	…
Bulk SPC				
Molecule	$\tau\mu$ (ps)		$\tau \perp \mu$ (ps)	
H_2O	3.2 ± 0.0		2.9 ± 0.0	
CH_3OH	2.9 ± 0.0		2.5 ± 0.0	
CH_3CH_2OH	3.0 ± 0.0		2.8 ± 0.0	

[a]Rotational relaxation time for the dipole vector.
[b]Rotational relaxation time for a perpendicular vector to the dipole.
[c]Rotational relaxation time for the collective dipole vector.
[d]Rotational relaxation time for a perpendicular vector to the collective dipole.
[e]No reliable estimate from MD simulations.

Quite interestingly, the dimeric to collective dipole transition is evidenced by the magnitudes of $\tau\vec{\mu}$ which are always smaller for the former case; indeed, for both the methanol-loaded and ethanol-loaded (7,7) and (8,8) pores, very few collective dipole flips were recorded during MD simulations, thus not allowing the calculations of $\tau\vec{\mu}$ or coll $\tau\vec{\mu}$ (see Fig. 11 of the supplementary material[47]). A further evidence of this strong dipolar alignment is reflected by the magnitude of the (single-file loaded) collective dipole vector, which for methanol are on average 7.7 ± 3.3 and 15 ± 1.1 D for (6,6) and (7,7) loaded tubes, respectively. Likewise the ethanol-loaded (6,6), (7,7), and (8,8) pores present values of 4.8 ± 1.8, 6.8 ± 2.7, and 23.1 ± 1.7 D, respectively. For completeness, the dipole for both ethanol and methanol in the current force field is of 1.91 D.

Last but not least, the collective configurations should present higher coll $\tau\vec{\mu}$ than $\tau\vec{\mu}$ (it is harder to flip a collective dipole than its individual components), this is the case for the (6,6) water-loaded tube. In fact, for water-loaded tubes, the tube-width increment renders coll $\tau\vec{\mu}$ smaller than $\tau\vec{\mu}$, an indication of the loss of correlations or collectiveness (see Table III). Regretfully, the impossibility to compute any τ for the methanol and ethanol loaded (7,7) and (8,8) pores precludes the same conclusions for alcohols; nevertheless, the behavior of the methanol-loaded (8,8) tube points towards this direction; despite it is not a rigorous single-file conformations, it contains two aligned dipoles (see Fig. 4). On the other hand, the local dipoles on the dimers are not necessarily aligned (see Fig. 4); thus, their values should be decoupled, and this seems to be case for all values shown in Table III.

IV. CONCLUSIONS

Methanol and ethanol partition by narrow SWCNTs has been thoroughly characterized via atomistic classical molecular dynamics simulations. For diluted solutions, the partitioning is very fast, normally in the order of 10 of ns, with selectivities generally proportional to the number of carbon atoms, as shown by others.[42] Structurally, all narrow tubes form single-files conformation, with a quite interesting passage from dipoles composed of two molecules to a single collective dipole that is pore-width dependent, we have termed the latter phenomena a dimeric to collective dipole transition. Energetic analyses evidenced that this transition is controlled by a fine balance between VdW interactions with the tube atoms and cooperative electrostatic interactions among the loaded particles. Mobility within the tubes is heavily hindered for alcohols with no substantial differences for either dimers or collective dipoles. Quite differently, the rotational dynamics presents a strong anisotropy between rotations parallel and perpendicular the dipole vector, both being substantially reduced for the collective systems.

The results presented in this work are a further step towards the understanding of nanofluidics, providing fundamental knowledge to support the design of nanoscale devices, in which a detailed atomistic characterization of nano-confinement effects is needed. We envision two types of applications: nano-filtering appliances for polar molecules and signal-amplification devices that can take advantage of the strong dipolar alignment; indeed, such constructs have been previously explored by other authors.[69–71]

Even though all evidence indicate that electrostatic interactions rising from nanotube polarization are rather weak,[65] the persistent dipoles formed by the collective arrangement of single-file alcohols, e.g., (7,7) methanol-loaded tube might lead to an instantaneous axial polarization of the tube, effect that is not accounted in our current model. We are currently implementing a polarizable carbon nanotube model that in conjunction with (an already developed) polarizable methanol force-field[68] will serve to assess polarization effects of confined alcohols within SWCNTs.

In future works, we plan to expand these studies by exploring the effects of tube functionalization, pressure driven fluxes and the response towards external electric fields. Moreover, we plan to fully describe the thermodynamical forces in alcohol partition by narrow pores, via rigorous free energy calculations.

ACKNOWLEDGMENTS

We thank Ignacio Fuenzalida for technical support in the implemetation of the KMC simulations. The authors acknowledge financial support from the Fondo Nacional de Desarrollo Científico y Tecnológico (FONDECYT) Project No. 3130547, Programa de Financiamiento Basal PFB16 Fundación Ciencia para la Vida, Project Nos. ACT-1107 PIA-CONICYT, and ICM-ECONOMIA P09-022-F. This research was partially supported by the supercomputing infrastructure of the NLHPC (ECM-02), Powered@NLHPC.

[1]S. Iijima, "Helical microtubules of graphitic carbon," Nature **354**, 56–58 (1991).
[2]B. J. Hinds, N. Chopra, T. Rantell, R. Andrews, V. Gavalas, and L. G. Bachas, "Aligned multiwalled carbon nanotube membranes," Science **303**, 62–65 (2004).
[3]J. H. Grossman and S. E. McNeil, "Nanotechnology in cancer medicine," Phys. Today **65**(8), 38 (2012).
[4]E. S. Snow, F. K. Perkins, E. J. Houser, S. C. Badescu, and T. L. Reinecke, "Chemical detection with a single-walled carbon nanotube capacitor," Science **307**, 1942–1945 (2005).
[5]E. Heister, V. Neves, C. Lamprecht, S. R. P. Silva, H. M. Coley, and J. McFadden, "Drug loading, dispersion stability, and therapeutic efficacy in targeted drug delivery with carbon nanotubes," Carbon **50**, 622–632 (2012).
[6]N.-T. N. Patrick Abgrall, *Nanofluidics* (Artech House, 2009).
[7]R. Singh, D. Pantarotto, L. Lacerda, G. Pastorin, C. Klumpp, M. Prato, A. Bianco, and K. Kostarelos, "Tissue biodistribution and blood clearance rates of intravenously administered carbon nanotube radiotracers," Proc. Natl. Acad. Sci. U. S. A. **103**, 3357–3362 (2006).
[8]A. Kalra, S. Garde, and G. Hummer, "Osmotic water transport through carbon nanotube membranes," Proc. Natl. Acad. Sci. U. S. A. **100**, 10175–10180 (2003).
[9]J.-A. Garate, N. J. English, and J. M. D. MacElroy, "Carbon nanotube assisted water self-diffusion across lipid membranes in the absence and presence of electric fields," Mol. Sim. **35**, 3–12 (2009).
[10]J. A. Garate, N. J. English, and J. M. D. MacElroy, "Static and alternating electric field and distance-dependent effects on carbon nanotube-assisted water self-diffusion across lipid membranes," J. Chem. Phys. **131**, 114508 (2009).
[11]J. S. Babu and S. P. Sathian, "The role of activation energy and reduced viscosity on the enhancement of water flow through carbon nanotubes," J. Chem. Phys. **134**, 194509 (2011).
[12]H. Verweij, M. C. Schillo, and J. Li, "Fast mass transport through carbon nanotube membranes," Small **3**, 1996–2004 (2007).

[13]M. Majumder, N. Chopra, and B. J. Hinds, "Mass transport through carbon nanotube membranes in three different regimes: Ionic diffusion and gas and liquid flow," ACS Nano **5**, 3867–3877 (2011).
[14]A. Berezhkovskii and G. Hummer, "Single-file transport of water molecules through a carbon nanotube," Phys. Rev. Lett. **89**, 64503 (2002).
[15]L. Maibaum and D. Chandler, "A coarse-grained model of water confined in a hydrophobic tube," J. Phys. Chem. B **107**, 1189–1193 (2003).
[16]J. Kofinger, G. Hummer, and C. Dellago, "A one-dimensional dipole lattice model for water in narrow nanopores," J. Chem. Phys. **130**, 154110 (2009).
[17]F. Zhu and K. Schulten, "Water and proton conduction through carbon nanotubes as models for biological channels," Biophys. J. **85**, 236–244 (2003).
[18]T. Remy, J. Cousin Saint Remi, R. Singh, P. A. Webley, G. V. Baron, and J. F. M. Denayer, "Adsorption and separation of C1-C8 alcohols on SAPO-34," J. Phys. Chem. C **115**, 8117–8125 (2011).
[19]U. Burghaus, D. Bye, K. Cosert, J. Goering, A. Guerard, E. Kadossov, E. Lee, Y. Nadoyama, N. Richter, E. Schaefer, J. Smith, D. Ulness, and B. Wymore, "Methanol adsorption in carbon nanotubes," Chem. Phys. Lett. **442**, 344–347 (2007).
[20]S. Wasi, S. Tabrez, and M. Ahmad, "Toxicological effects of major environmental pollutants: An overview," Environ. Monit. Assess. **185**, 2585 (2013).
[21]C. Xue, G.-Q. Du, L.-J. Chen, J.-G. Ren, J.-X. Sun, F.-W. Bai, and S.-T. Yang, "A carbon nanotube filled polydimethylsiloxane hybrid membrane for enhanced butanol recovery," Sci. Rep. **4**, 5925 (2014).
[22]M. C. Ncibi and M. Sillanpää, "Optimized removal of antibiotic drugs from aqueous solutions using single, double and multi-walled carbon nanotubes," J. Hazard. Mater. **298**, 102–110 (2015).
[23]J. A. Garate, T. Perez-Acle, and C. Oostenbrink, "On the thermodynamics of carbon nanotube single-file water loading: Free energy, energy and entropy calculations," Phys. Chem. Chem. Phys. **16**, 5119–5128 (2014).
[24]M. C. Gordillo and J. Martí, "Hydrogen bond structure of liquid water confined in nanotubes," Chem. Phys. Lett. **329**, 341–345 (2000).
[25]G. Hummer, J. C. Rasaiah, and J. P. Noworyta, "Water conduction through the hydrophobic channel of a carbon nanotube," Nature **414**, 188–190 (2001).
[26]A. Alexiadis and S. Kassinos, "Molecular simulation of water in carbon nanotubes," Chem. Rev. **108**, 5014 (2008).
[27]J. Kofinger, G. Hummer, and C. Dellago, "Single-file water in nanopores," Phys. Chem. Chem. Phys. **13**, 15403–15417 (2011).
[28]N. Naguib, H. Ye, Y. Gogotsi, A. G. Yazicioglu, C. M. Megaridis, and M. Yoshimura, "Observation of water confined in nanometer channels of closed carbon nanotubes," Nano Lett. **4**, 2237–2243 (2004).
[29]H.-J. Wang, X.-K. Xi, A. Kleinhammes, and Y. Wu, "Temperature-induced hydrophobic-hydrophilic transition observed by water adsorption," Science **322**, 80–83 (2008).
[30]S. Cambré and W. Wenseleers, "Separation and diameter-sorting of empty (end-capped) and water-filled (open) carbon nanotubes by density gradient ultracentrifugation," Angew. Chem. **50**, 2764–2768 (2011).
[31]S. Vaitheeswaran, J. C. Rasaiah, and G. Hummer, "Electric field and temperature effects on water in the narrow nonpolar pores of carbon nanotubes," J. Chem. Phys. **121**, 7955–7965 (2004).
[32]T. A. Pascal, W. A. Goddard, and Y. Jung, "Entropy and the driving force for the filling of carbon nanotubes with water," Proc. Natl. Acad. Sci. U. S. A. **108**, 11794–11798 (2011).
[33]A. Waghe, J. C. Rasaiah, and G. Hummer, "Entropy of single-file water in (6,6) carbon nanotubes," J. Chem. Phys. **137**, 44709 (2012).
[34]H. Kumar, C. Dasgupta, and P. K. Maiti, "Driving force of water entry into hydrophobic channels of carbon nanotubes: Entropy or energy?," Mol. Simul. **41**, 504–511 (2015).
[35]P. Sahu, S. M. Ali, and K. T. Shenoy, "Thermodynamics of fluid conduction through hydrophobic channel of carbon nanotubes: The exciting force for filling of nanotubes with polar and nonpolar fluids," J. Chem. Phys. **142**, 074501 (2015).
[36]A. Kalra, G. Hummer, and S. Garde, "Methane partitioning and transport in hydrated carbon nanotubes," J. Phys. Chem. B **108**, 544–549 (2004).
[37]J. Zheng, E. M. Lennon, H. K. Tsao, Y. J. Sheng, and S. Jiang, "Transport of a liquid water and methanol mixture through carbon nanotubes under a chemical potential gradient," J. Chem. Phys. **122**, 214702 (2005).
[38]L. Yang and Y. Q. Gao, "Effects of cosolvents on the hydration of carbon nanotubes," J. Am. Chem. Soc. **132**, 842–848 (2010).
[39]Y. Liu, S. Consta, and W. A. Goddard, "Nanoimmiscibility: Selective absorption of liquid methanol-water mixtures in carbon nanotubes," J. Nanosci. Nanotechnol. **10**, 3834–3843 (2010).
[40]S.-p. Du, W.-h. Zhao, and L.-f. Yuan, "Absorption and structural property of ethanol/water mixture with carbon nanotubes," Chin. J. Chem. Phys. **25**, 487 (2012).
[41]W. H. Zhao, B. Shang, S. P. Du, L. F. Yuan, J. Yang, and X. C. Zeng, "Highly selective adsorption of methanol in carbon nanotubes immersed in methanol-water solution," J. Chem. Phys. **137**, 034501 (2012).
[42]X. Tian, Z. Yang, B. Zhou, P. Xiu, and Y. Tu, "Alcohol-induced drying of carbon nanotubes and its implications for alcohol/water separation: A molecular dynamics study," J. Chem. Phys. **138**, 204711 (2013).
[43]I. Yzeiri, N. Patra, and P. Král, "Porous carbon nanotubes: Molecular absorption, transport, and separation," J. Chem. Phys. **140**, 104704 (2014).
[44]A. D. MacKerell, D. Bashford, M. Bellott, R. L. Dunbrack, J. D. Evanseck, M. J. Field, S. Fischer, J. Gao, H. Guo, S. Ha, D. Joseph-McCarthy, L. Kuchnir, K. Kuczera, F. T. K. Lau, C. Mattos, S. Michnick, T. Ngo, D. T. Nguyen, B. Prodhom, W. E. Reiher, B. Roux, M. Schlenkrich, J. C. Smith, R. Stote, J. Straub, M. Watanabe, J. Wiorkiewicz-Kuczera, D. Yin, and M. Karplus, "All-atom empirical potential for molecular modeling and dynamics studies of proteins," J. Phys. Chem. B **102**, 3586–3616 (1998).
[45]W. D. Cornell, P. Cieplak, C. I. Bayly, I. R. Gould, K. M. Merz, D. M. Ferguson, D. C. Spellmeyer, T. Fox, J. W. Caldwell, and P. A. Kollman, "A second generation force field for the simulation of proteins, nucleic acids, and organic molecules," J. Am. Chem. Soc. Vol. **117**, 5179–5197 (1995); e-print arXiv:z0024 .
[46]R. D. Lins and P. H. Hunenberger, "A new GROMOS force field for hexopyranose-based carbohydrates," J. Comput. Chem. **26**, 1400–1412 (2005).
[47]See supplementary material at http://dx.doi.org/10.1063/1.4941331 for extra figures about the tube rigidity, water and methane density profiles, water content in alcohol-loaded tubes, h-bonds, removed energy terms from fig. 6, energy terms for water and methane, additional displacement correlation calculations, distribution and time series of P1 and detailed parameters employed in this work.
[48]S. G. Srinivasan, A. C. T. van Duin, and P. Ganesh, "Development of a reaxff potential for carbon condensed phases and its application to the thermal fragmentation of a large fullerene," J. Phys. Chem. A **119**, 571–580 (2015).
[49]B. D. Jensen, K. E. Wise, and G. M. Odegard, "Simulation of the elastic and ultimate tensile properties of diamond, graphene, carbon nanotubes, and amorphous carbon using a revised reaxff parametrization," J. Phys. Chem. A **119**, 9710–9721 (2015).
[50]J.-P. Ryckaert, G. Ciccotti, and H. J. C. Berendsen, "Numerical integration of the cartesian equations of motion of a system with constraints: Molecular dynamics of n-alkanes," J. Comput. Phys. **23**, 327 (1977).
[51]T. Werder, J. H. Walther, R. L. Jaffe, T. Halicioglu, and P. Koumoutsakos, "On the water—carbon interaction for use in molecular dynamics simulations of graphite and carbon nanotubes," J. Phys. Chem. B **107**, 1345–1352 (2003).
[52]N. Schmid, C. D. Christ, M. Christen, A. P. Eichenberger, and W. F. van Gunsteren, "Architecture, implementation and parallelisation of the GROMOS software for biomolecular simulation," Comput. Phys. Commun. **183**, 890–903 (2012).
[53]S. Riniker, C. D. Christ, H. S. Hansen, P. H. Hunenberger, C. Oostenbrink, D. Steiner, and W. F. van Gunsteren, "Calculation of relative free energies for ligand-protein binding, solvation, and conformational transitions using the gromos software," J. Phys. Chem. B **115**, 13570–13577 (2011).
[54]R. W. Hockney, "The potential calculation and some applications," Methods Comput. Phys. **9**, 136–211 (1977).
[55]I. G. Tironi, R. Sperb, P. E. Smith, and W. F. van Gunsteren, "A generalized reaction field method for molecular dynamics simulations," J. Chem. Phys. **102**, 5451–5459 (1995).
[56]S. Nose, "A unified formulation of the constant temperature molecular dynamics methods," J. Chem. Phys. **81**, 511–519 (1984).
[57]W. G. Hoover, "Canonical dynamics: Equilibrium phase-space distributions," Phys. Rev. A **31**, 1695–1697 (1985).
[58]M. P. Allen and D. J. Tildesley, *Computer Simulations of Liquids* (Oxford Science Publications, 1987).
[59]P. Liu, E. Harder, and B. J. Berne, "On the calculation of diffusion coefficients in confined fluids and interfaces with an application to the liquidvapor interface of water," J. Phys. Chem. B **108**, 6595–6602 (2004).
[60]A. Striolo, "The mechanism of water diffusion in narrow carbon nanotubes," Nano Lett. **6**, 633–639 (2006).
[61]B. Mukherjee, P. K. Maiti, C. Dasgupta, and A. K. Sood, "Strong correlations and Fickian water diffusion in narrow carbon nanotubes," J. Chem. Phys. **126**, 124704 (2007).
[62]P. Drude, *The Theory of Optics* (Milikan, Longmans, Green and Co., New York, 1987), Vol. 1902.

[63]G. Lamoureux and B. Roux, "Modeling induced polarization with classical Drude oscillators: Theory and molecular dynamics simulation algorithm," J. Chem. Phys. **119**, 3025–3039 (2003).
[64]Y. Xie, Y. Kong, H. Gao, and A. Soh, "Molecular dynamics simulation of polarizable carbon nanotubes," Comput. Mater. Sci. **40**, 460–465 (2007).
[65]F. Moulin, M. Devel, and S. Picaud, "Molecular dynamics simulations of polarizable nanotubes interacting with water," Phys. Rev. B: Condens. Matter Mater. Phys. **71**, 165401 (2005).
[66]T. A. Ho and A. Striolo, "Polarizability effects in molecular dynamics simulations of the graphene-water interface," J. Chem. Phys. **138**, 054117 (2013).
[67]Z. E. Hughes, S. M. Tomasio, and T. R. Walsh, "Efficient simulations of the aqueous bio-interface of graphitic nanostructures with a polarisable model," Nanoscale **6**, 5438–5448 (2014).
[68]H. Yu, D. P. Geerke, H. Liu, and W. F. Van Gunsteren, "Molecular dynamics simulations of liquid methanol and methanol-water mixtures with polarizable models," J. Computat. Chem. **27**, 1494–1504 (2006).
[69]Y. Tu, P. Xiu, R. Wan, J. Hu, R. Zhou, and H. Fang, "Water-mediated signal multiplication with Y-shaped carbon nanotubes," PNAS **106**, 18120–18124 (2009).
[70]Y. Tu, H. Lu, Y. Zhang, T. Huynh, and R. Zhou, "Capability of charge signal conversion and transmission by water chains confined inside Y-shaped carbon nanotubes," J. Chem. Phys. **138**, 015104 (2013).
[71]M. Lv, B. He, Z. Liu, P. Xiu, and Y. Tu, "Charge-signal multiplication mediated by urea wires inside Y-shaped carbon nanotubes," J. Chem. Phys. **141**, 044707 (2014).